Successive Dimensional Transition in $(TMTTF)_2PF_6$ Revealed by Synchrotron X-ray Diffraction

Shunsuke Kitou,[1] Tatsuya Fujii,[1] Tadashi Kawamoto,[2] Naoyuki Katayama,[1] Sachiko Maki,[1,†] Eiji Nishibori,[1,‡]
Kunihisa Sugimoto,[3] Masaki Takata,[4] Toshikazu Nakamura,[5] and Hiroshi Sawa[1,*]

[1]*Department of Applied Physics, Nagoya University, Nagoya 464-8603, Japan*
[2]*Department of Materials Science and Engineering, Tokyo Institute of Technology,
O-okayama, Meguro-ku, Tokyo 152-8552, Japan*
[3]*Japan Synchrotron Radiation Research Institute (JASRI), SPring-8, Hyogo 679-5198, Japan*
[4]*Institute of Multidisciplinary Research for Advanced Materials, Tohoku University, Sendai 980-8577, Japan*
[5]*Institute for Molecular Science, Myodaiji, Okazaki, 444-8585, Japan*

A quasi-one-dimensional organic charge-transfer salt $(TMTTF)_2PF_6$ undergoes a multistep phase transition as the temperature decreases. One of these transitions is called a "structureless transition," and these detailed structures were unknown for many years. With synchrotron x-ray diffraction, we observed a slight structural difference owing to the effect of charge-order transition between two TMTTF molecules in a dimer, which corresponds to the charge transfer $\delta_{CO} = 0.20e$. The two-dimensional Wigner crystallization was determined from an electron density analysis using core differential Fourier synthesis. Furthermore, we found that the ground state due to tetramerization, called the spin Peierls phase, is a three-dimensional transition with interchain correlation.

Molecular conductors exhibit various electronic states because the quantum parameters (transition integrals and electronic correlation energies) of substances are small and antagonistic. However, it is difficult to accurately identify various order parameters reflecting small energy scales. The modeling of a one-dimensional (1D) chain 1/4 filled by the extended Hubbard Hamiltonian with a dimerized molecule as a unit can explain many physical properties fairly well [1]. However, to clarify the ground state, it is necessary to consider competing or cooperating order parameters. For example, in the quasi-1D system $(DI-DCNQI)_2Ag$, the hybrid of the charge-order (CO) state and the bond order wave state in the unit cell dissolves the inherent spiral frustration [2–4]. To discuss the physical properties of molecular crystals, it is important to obtain the information of a precise crystal structure and charge distribution states.

The rich (physical and chemical) pressure-temperature (P-T) phase diagram of the organic charge-transfer salt $(TMTCF)_2X$ (C denotes S or Se and X^- denotes a monovalent anion) [5–7], which consists of weak dimers of TMTCF stacked in the a-axis direction [8], commonly reflects the low-dimensional electronic properties and relatively strong electron-electron correlations [9]. In these salts, the TMTTF ($C =$ S) is a tetramethyltetrathiofulvalene, and X is PF_6, AsF_6, ReO_4, SCN, I, etc. To understand the various electronic states formed by this system, the metallic, semiconducting, CO, antiferromagnetic, and spin Peierls phases [10–12], pressure-dependent transport measurements [6,13], optical, and NMR, and ESR spectroscopy [14–17], or x-ray and neutron scattering experiments have been conducted [18,19]. Nevertheless, the nature of the ground states and the interplay of the different degrees of freedom (d.o.f.) are not completely understood.

Here we focused on $(TMTTF)_2PF_6$ which shows a multistep phase transition to the metal state, the dimer Mott insulator, the CO phase, and the spin Peierls phase under the ambient pressure. Although structural studies have been performed mostly from various viewpoints among this series of systems, sufficient information was not obtained from a crystallographic point of view for a long time.

The transition from the dimer Mott phase to the CO phase at approximately 67 K is called a mysterious "structureless transition" because the structural parameters were very nearly consistent across the transition. Some experiments tried to elucidate this mystery [20–22]. This charge ordering implies the disappearance of the d.o.f. of the charge distribution in the dimer and suggests that the electronic correlation is multilayered [23]. By further decreasing the temperature, a nonmagnetic transition appears at 19 K [24,25]. It is believed that a spin Peierls ground state occurs because it has a 1D crystal structure. Although the emergence of superlattice structures has already been reported, reliable structural refinements have never been performed owing to the extremely weak superlattice peaks [18,19].

In this Letter, we report synchrotron x-ray diffraction structural studies of $(TMTTF)_2PF_6$. We successfully estimated the magnitude of the charge disproportionation in the CO phase and observed the tetramerization of TMTTF molecules in the spin Peierls phase by a very careful structural analysis using high-quality data obtained by synchrotron x rays.

Synchrotron x-ray diffraction experiments were performed with the BL02B1 beam line equipped at SPring-8, Japan. Two single-crystal samples with different sizes were used in the experiments. A small sample with dimensions of $100 \times 80 \times 50$ μm^3 was used for the measurements at 100 (the dimer Mott phase) and 30 K (the CO phase). A large sample with dimensions of $350 \times 250 \times 100$ μm^3 was used for the measurement at 7 K (the spin Peierls phase). Although a He-gas-blowing device was used for measurements at 100 and 30 K, a refrigerator was used for measurements at 7 K. The diffraction experiments were performed using synchrotron x rays with an incident energy of $E = 35$ keV. A large imaging plate was used as the diffractometer's detector. For the analysis, we used original software for extracting the peak intensity. Peak-intensity averaging, a structural analysis, and a Bader's topological analysis were performed using SORTAV [26], Jana2006 [27], and TOPOXD [28], respectively.

The results of the structural analyses at 100, 30, and 7 K are shown in the Supplemental Material [29]. To obtain accurate atomic positions and observe the amount of charge transfer in the CO phase, we performed a high-angle analysis and core differential Fourier synthesis (CDFS) analysis as described below. The former analysis used only high-angle reflections that were not affected by valence electrons [30]. The latter analysis could obtain the electron density of a molecular orbital with little truncation effect of the inverse Fourier transform.

In the dimer Mott phase, the space group is $P\bar{1}$, which is the same as that in the metallic state. Owing to the large thermal oscillations, it is not possible to obtain the intensity of the reflections in the high angle region with a sufficient accuracy to obtain the atomic position. Therefore, structural refinement was performed using the total reflections. The number of observed unique reflections was 20 909 in the resolution limit of $d > 0.4$ Å. The R value was R_1 $(I > 4\sigma) =$ 3.28% (the number of unique reflections: 14 098).

In the CO phase, the space group becomes $P1$ with the loss of the inversion center, and the crystal structure includes merohedral twins. The ratio of twins can be obtained using twinning matrices by extracting the difference in the amount of charge between dimers, i.e., the difference in the bond length. If a TMTTF molecule with $0.5|e|$ becomes hole poor ($<0.5|e|$) by charge transfer, the bond length of the bonding orbital on C=C becomes shorter, and the antibonding orbital on C–S becomes longer. If it becomes hole rich ($>0.5|e|$), C=C becomes longer, and C–S becomes shorter.

First, we performed an analysis using the total reflections ($d > 0.35$ Å). The R value was $R_1(I > 4\sigma) = 2.69\%$ (37 565). However, we did not observe a systematic difference in the bond length corresponding to charge transfer.

Next, we performed a high-angle analysis using only 0.35 Å $< d < 1$ Å reflections. The R value was $R_1(I > 3\sigma) = 2.32\%$ (31 945), and we could observe a difference in the bond length corresponding to charge transfer. The ratio of the merohedral twins was 8 : 2. Detailed analysis results and the bond length are shown in the Supplemental Material [29]. The amount of charge transfer empirically calculated
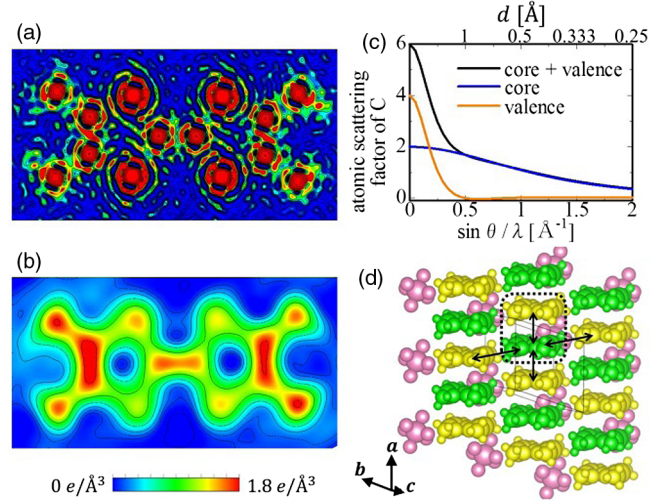

FIG. 1.   (a) and (b) All electron density distribution and valence electron density distributions of the TMTTF molecule 1 (hole poor), respectively. (c) Atomic scattering factor of carbon [27]. The blue, orange, and black lines indicate the contributions of the core, valence, and total electrons, respectively. (d) CO patterns of hole-rich and hole-poor (yellow and green) molecules, which indicate a 2D Wigner crystal state. The region surrounded by a dotted line shows a TMTTF molecule dimer.

from the bond length of the TMTTF molecule was $\delta_{CO} = 0.17e$ (the difference in the amount of charge between two molecules is $0.34e$) [31]. We calculated the highest occupied molecular orbital (HOMO) levels of TMTTF molecules by the extended Hückel method using these structural parameters [32], and it was confirmed that TMTTF molecule 1 (hole poor) was 21.7 meV lower than molecule 2 (hole rich). These results show that the high-angle analysis gives the correct structure factor parameters.

Figure 1(a) shows the total electron density distribution of TMTTF molecule 1 calculated by a normal inverse Fourier transform. The truncation effect due to the inverse Fourier transform appears remarkably around atoms. Figure 1(c) shows the atomic scattering factor of carbon [27]. Since the total atomic scattering factor (core + valence) of the minimum d value used for the analysis is not zero, the waviness in the electron density around the atoms in Fig. 1(a) occurs. To suppress this effect, we performed the CDFS analysis using the atomic positions and the thermal vibration parameters obtained by the high-angle analysis.

Figure 1(b) shows the valence electron density distribution of TMTTF molecule 1 obtained by the CDFS method. Both the smooth electron density of the bonding orbital on the C=C bond and the electron density node of the antibonding orbital of the C–S bond are clearly shown.

The method of the CDFS analysis is described as

$$\rho_v(\boldsymbol{r}) = \frac{1}{V} \sum_{\boldsymbol{K}} \left[\left(|F_{\text{obs}}(\boldsymbol{K})| - \left| \sum_j f_j^{\text{core}} T_j e^{-i\boldsymbol{K} \cdot \boldsymbol{r}_j} \right| \right) P e^{i\boldsymbol{K} \cdot \boldsymbol{r}} \right],$$

(1)

where $\rho_v(\boldsymbol{r})$ is the electron density of the molecular orbital, V is the cell volume, and $\boldsymbol{r}_j$ is the jth atomic position in a unit cell. $F_{\mathrm{obs}}(\boldsymbol{K})$ is the observed crystal structure factor, f_j^{core} is the jth core atomic scattering factor [i.e., the blue line in Fig. 1(c)], T_j is the jth thermal vibration parameters, and P is the phase term.

This is a method of extracting the electron density of a molecular orbital by an inverse Fourier transformation using the crystal structure factor of only the valence electron term. As shown in Fig. 1(c), the high-angle part of the atomic scattering factor is only the contribution of the core electrons. The phase term P of the crystal structure factor can be precisely obtained by refining the atomic positions $\boldsymbol{r}_j$ and the thermal vibration parameters T_j of the constructed atoms by using the high-angle reflections intensity. Using these phase terms, inverse Fourier transformation is performed using the crystal structure factor of only the valence electron term obtained by subtracting the calculated crystal structure factor using the core atomic scattering factor from the observed crystal structure factor $F_{\mathrm{obs}}(\boldsymbol{K})$. By using this method, a smooth electron density of the molecular orbital can be reconstructed.

This method can be applied to the determination of molecular orbitals in molecular crystals and to the localized d orbitals of transition metals in inorganic crystals, which is a unique way to discuss more detailed electronic states.

By comparing the valence electron number of the two TMTTF molecules in the dimer obtained by the CDFS analysis in the atomic basins calculated by the Bader's topological analysis, the amount of charge transfer was $\delta_{\mathrm{CO}} = 0.20e$. This value is consistent with $\delta_{\mathrm{CO}} = 0.14e$ of the NMR experiment [16]. We directly revealed that the spatial CO pattern formed a 2D Wigner crystal state from both the molecular structure and the electron density distribution in the CO phase called a structureless transition [Fig. 1(d)]. This is also consistent with past ESR experiments [17], and theoretical expectations [33–35].

In the spin Peierls phase, a superlattice reflection of $\boldsymbol{q} = (1/2, 1/2, 1/2)$ was observed. Figure 2(a) shows x-ray diffraction data at 7 K. In the general spin Peierls transition such as that for CuGeO$_3$ [36], a diffuse scattering appears owing to a weak interchain correlation, but in (TMTTF)$_2$PF$_6$, no diffuse scattering was observed even just above the spin Peierls transition temperature. The integrated intensity of the superlattice reflections is very weak, which is approximately 4 orders of magnitude lower than the fundamental reflections intensity. After expanding the unit lattice to $2\boldsymbol{a} \times 2\boldsymbol{b} \times 2\boldsymbol{c}$, there exists an F lattice extinction rule in which the intensity does not appear with not odd numbered reflections for all h, k, and l in the superlattice reflections. Therefore, we virtually made the space group $F1$, which is not described in the international table. This F lattice extinction rule reflects the correlation among the chains of TMTTF molecules. The actual primitive unit cell with $1/4$ volume is defined by the
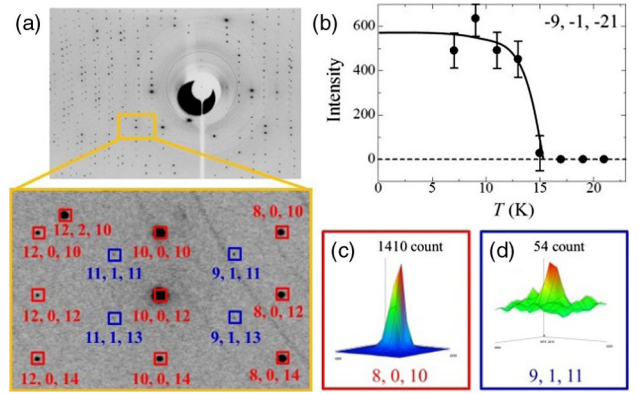

FIG. 2.   (a) X-ray diffraction data at 7 K; the all-even and all-odd indices indicate fundamental and superlattice reflections, respectively. (b) Temperature dependence of the integrated intensity of the superlattice reflection $(-9, -1, -21)$. (c) and (d) peak profiles of the fundamental and superlattice reflections, which are indicated on the same scale as the background.

following three vectors: $\boldsymbol{a}_p = (2\boldsymbol{a} + 2\boldsymbol{b})/2$, $\boldsymbol{b}_p = (2\boldsymbol{b} + 2\boldsymbol{c})/2$, and $\boldsymbol{c}_p = (2\boldsymbol{c} + 2\boldsymbol{a})/2$. For simplicity, the following explanation will proceed with an F lattice of $2\boldsymbol{a} \times 2\boldsymbol{b} \times 2\boldsymbol{c}$. Figure 2(b) shows the temperature dependence of the integrated intensity of a $(-9, -1, -21)$ superlattice reflection, and (c) and (d) show the peak profiles of the fundamental reflection and the superlattice reflection shown at the same scale. The superlattice reflections appears below 15 K, and its full width at half maximum is comparable to that of the fundamental reflections. Since this means that the coherence length of the superlattice is up to the resolution limit, we can carry out an analysis including the superlattice peaks.

In the spin Peierls phase, we could not perform structural refinement using the full matrix least-squares method owing to complex problems around the low completeness and weak superlattice reflections. The equipment restrictions due to the refrigerator strongly lowered the accessible superlattice reflections to 20.8% of all reflections with $d > 0.8$ Å (2810). Furthermore, many superlattice reflections were excluded under the restriction of $I > 1.5\sigma$, resulting in only 51 superlattice reflections available for refinement. For performing structural refinement using a limited number of superlattice reflections, only the positions and directions of the TMTTF and PF$_6$ molecules were refined by assuming that they were rigid bodies. Owing to the restrictions of the $F1$ triclinic lattice, the primitive cell of this phase is twice that of the original unit cell. The crystallographically independent TMTTF and PF$_6$ molecules in this unit cell are four and two, respectively. As the result of refinement, the displacements of the TMTTF molecules were identified with an order of 0.01 Å along the a- and c-axis directions. The resulting arrangements of TMTTF molecules suggest the emergence of TMTTF tetramerization. The details of the obtained molecular
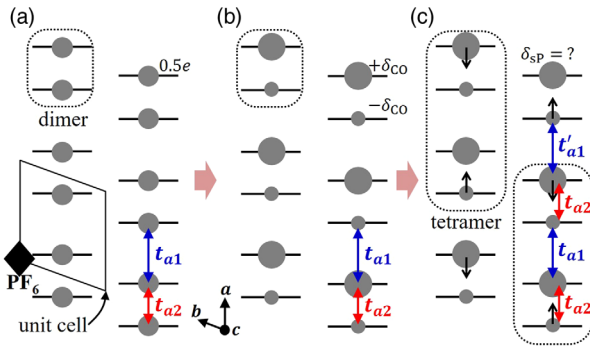
FIG. 3.   Schematic configuration along the molecular stacking direction for $(TMTTF)_2PF_6$: (a) dimer Mott, (b) CO, and (c) spin Peierls phases. Large (small) circles denote hole-rich (hole-poor) TMTTF molecules. The black arrows on the circles show the molecular displacement corresponding to tetramerization.

displacement are summarized in the Supplemental Material [29].

In the transition from the CO phase to the spin Peierls phase, superlattice reflections implying a clear phase transition appear. Owing to the TMTTF molecule shift, tetramers formed along the 1D chain direction. Since the phase of the arrangement of the tetramers shifted by π among the chains, a 3D F lattice formed, and the lattice distortion became uniform. Considering the 3/4-filled band configurations, it can be easily understood that the spin Peierls ground state was achieved alongside tetramerization.

A schematic configuration from the dimer Mott phase to the CO and spin Peierls phases is shown in Fig. 3. Molecular orbital and transfer integrals were calculated by the extended Hückel method using the structural parameters in the dimer Mott, CO, and spin Peierls phases [32]. When comparing the ratio of intradimer transfer t_{a2} to interdimer transfer t_{a1} in each phase, t_{a2}/t_{a1} (and t_{a2}/t'_{a1} in the spin Peierls phase) became 1.15 (Mott), 1.13 (CO), and 1.16 and 1.20 (spin Peierls). There were two cases of narrowing and spreading between the dimers in the spin Peierls phase [Fig. 3(c)]. The dimerization in the spin Peierls phase is stronger than that in the dimer Mott and CO phases. This is the cause of tetramerization in the spin Peierls phase. It seems that the spin Peierls state was formed by the increasing charge localization of the intradimer.

The charge d.o.f.'s involvement in the phase transition from the CO phase to the spin Peierls phase is interesting. For example, since it is noteworthy that $(TMTTF)_2I$ directly transfers to the spin Peierls phase without passing through the CO phase [37], there is no charge disproportionation in the spin Peierls ground state. In our experiments, however, the charge distribution in the spin Peierls phase could not be accurately obtained owing to poor data quality. Although we calculated t_{a2}/t_{a1} and t_{a2}/t'_{a1} assuming that the CO pattern was flat or ferroelectric (o–O o–O) in the spin Peierls phase (o denotes hole poor, O denotes hole rich), there was no difference in these two values.

The ferroelectric transfer integrals were virtually calculated using TMTTF molecules in the CO phase. This result means that the CO pattern of the intradimer and the TMTTF molecular displacement dominates this ground state. Because it is unlikely that this inversion symmetry will be restored by this phase transition, we expect that the CO pattern is ferroelectric, which is the same as the CO phase, and this pattern is consistent with the results obtained by Raman spectroscopy [38].

In summary, we conducted synchrotron x-ray diffraction experiments on $(TMTTF)_2PF_6$ with a quasi-1D structure. In the CO transition called a structureless transition, the charge transfer between the dimers was directly measured from the electron density analysis, which revealed that the CO pattern formed a 2D Wigner crystal state in real space. In the spin Peierls phase, it was found that the superlattice reflections pattern satisfies the symmetry of the F lattice. A structural analysis including superlattice reflections revealed that TMTTF molecules are tetramerized in the 1D chain direction, and the system is 3D ordered with a phase shift of π between the chains by the correlation among the chains of TMTTF molecules. It seems that the dimensionality of the electronic state undergoes a multistep change during the phase transition of this system.

*Corresponding author.
z47827a@cc.nagoya-u.ac.jp
†Present address: Graduate School of Science, Hiroshima University, 1-3-1 Kagamiyama, Higashi-Hiroshima 739-8526, Japan.
‡Present address: Faculty of Pure and Applied Sciences, Center for Integrated Research in Fundamental Science and Engineering (CiRfSE), and Tsukuba Research Center for Interdisciplinary Materials Science (TIMS), University of Tsukuba, Tsukuba, Ibaraki 305-8571, Japan.

[1] H. Seo, C. Hotta, and H. Fukuyama, Chem. Rev. **104**, 5005 (2004).
[2] K. Hiraki and K. Kanoda, Phys. Rev. Lett. **80**, 4737 (1998).
[3] T. Kakiuchi, Y. Wakabayashi, H. Sawa, T. Itou, and K. Kanoda, Phys. Rev. Lett. **98**, 066402 (2007).
[4] H. Seo and Y. Motome, Phys. Rev. Lett. **102**, 196403 (2009).
[5] D. Jérome, Science **252**, 1509 (1991).
[6] B. Köhler, E. Rose, M. Dumm, G. Untereiner, and M. Dressel, Phys. Rev. B **84**, 035124 (2011).
[7] F. Iwase, K. Sugiura, K. Furukawa, and T. Nakamura, Phys. Rev. B **84**, 115140 (2011).
[8] J. L. Galigne, B. Liautard, S. Peytavin, G. Brun, J. M. Fabre, E. Torreills, and L. Giral, Acta Crystallogr. Sect. B **34**, 620 (1978).

[9] P. Monceau, F. Ya. Nad, and S. Brazovskii, Phys. Rev. Lett. **86**, 4080 (2001).

[10] D. Jérome, A. Mazaud, M. Ribanult, and K. Bechgaard, J. Phys. (Paris), Lett. **41**, 95 (1980).

[11] D. Jérome, Solid State Commun. **92**, 89 (1994).

[12] D. Jérome, P. AubanSenzier, L. Balicas, K. Behnia, W. Kang, P. Wzietek, C. Berthier, P. Caretta, M. Horvatic, P. Segransa, L. Hubert, and C. Bourbonnais, Synth. Met. **70**, 719 (1995).

[13] V. Vescoli, L. Degiorgi, W. Henderson, G. Grüner, K. P. Starkey, and L. K. Montgomery, Science **281**, 1181 (1998).

[14] C. S. Jacobsen, D. B. Tanner, and K. Bechgaard, Phys. Rev. B **28**, 7019 (1983).

[15] D. S. Chow, F. Zamborszky, B. Alavi, D. J. Tantillo, A. Baur, C. A. Merlic, and S. E. Brown, Phys. Rev. Lett. **85**, 1698 (2000).

[16] T. Nakamura, K. Furukawa, and T. Hara, J. Phys. Soc. Jpn. **76**, 064715 (2007).

[17] T. Nakamura, J. Phys. Soc. Jpn. **72**, 213 (2003).

[18] J.-P. Pouget, R. Moret, R. Comes, K. Bechgaard, J. M. Fabre, and L. Giral, Mol. Cryst. Liq. Cryst. **79**, 485 (1982).

[19] P. Foury-Leylekian, D. Le Bolloc'h, B. Hennion, S. Ravy, A. Moradpour, and J.-P. Pouget, Phys. Rev. B **70**, 180405 (2004).

[20] C. Coulon, S. S. P. Parkin, and R. Laversanne, Phys. Rev. B **31**, 3583 (1985).

[21] M. de Souza, P. Foury-Leylekian, A. Moradpour, J.-P. Pouget, and M. Lang, Phys. Rev. Lett. **101**, 216403 (2008).

[22] P. Foury-Leylekian, S. Petit, G. Andre, A. Moradpour, and J.-P. Pouget, Physica (Amsterdam) **405B**, S95 (2010).

[23] F. Nad, P. Monceau, C. Carcel, and J. M. Fabre, Phys. Rev. B **62**, 1753 (2000).

[24] S. Flandrois, C. Coulon, P. Delhaes, D. Chasseau, C. Hauw, J. Gaultter, J. M. Fabre, and L. Giral, Mol. Cryst. Liq. Cryst. **79**, 663 (1982).

[25] M. Dumm, A. Loidl, B. W. Fravel, K. P. Starkey, L. K. Montgomery, and M. Dressel, Phys. Rev. B **61**, 511 (2000).

[26] R. H. Blessing, Crystallography Reviews **1**, 3 (1987).

[27] V. Petříček, M. Dušek, and L. Palatinus, Z. Kristallogr. Cryst. Mater. **229**, 345 (2014).

[28] A. Volkov, P. Macchi, L. J. Farrugia, C. Gatti, P. Mallinson, T. Richter, and T. Koritsanszky, XD2016, a computer program package for multipole refinement, topological analysis of charge densities and evaluation of intermolecular energies from experimental or theoretical structure factors, 2016.

[29] See Supplemental Material at http://link.aps.org/supplemental/10.1103/PhysRevLett.119.065701 for lattice parameters, summary of refinement data, the result of high angle analysis, and magnitude of the molecule displacements in the spin Peierls state.

[30] S. Pillet, M. Souhassou, C. Lecomte, k. Schwarz, P. Blaha, M. Rérat, A. Lichanot, and P. Roversi, Acta Crystallogr. Sect. A **57**, 290 (2001).

[31] T. C. Umland, S. Allie, T. Kuhimann, and P. Coppens, J. Phys. Chem. **92**, 6456 (1988).

[32] T. Mori, A. Kobayashi, Y. Sasaki, H. Kobayashi, G. Saito, and H. Inokuchi, Bull. Chem. Soc. Jpn. **57**, 627 (1984).

[33] H. Seo and H. Fukuyama, J. Phys. Soc. Jpn. **66**, 1249 (1997).

[34] S. Mazumdar, R. T. Clay, and D. K. Campbell, Phys. Rev. B **62**, 13400 (2000).

[35] Y. Shibata, S. Nishimoto, and Y. Ohta, Phys. Rev. B **64**, 235107 (2001).

[36] J. P. Schoeffel, J.-P. Pouget, G. Dhalenne, and A. Revcolevschi, Phys. Rev. B **53**, 14971 (1996).

[37] K. Furukawa, K. Sugiura, F. Iwase, and T. Nakamura, Phys. Rev. B **83**, 184419 (2011).

[38] R. Świetlik and M. Dressel, Phys. Rev. B **95**, 085205 (2017).